Jornadas de Automática

Neuromorphic Automatic Reset PI Controller for Simultaneous Anti-Windup and Dead-Zone Compensation: Initial Results

Andrés J. Serrano-Balbontín*, Enrique Mancha-Sánchez, Inés Tejado, Blas M. Vinagre

Escuela de Ingenierías Industriales, Universidad de Extremadura, 06006 Badajoz, España.

To cite this article: Serrano-Balbontín, A.J., Mancha-Sánchez, E., Tejado, I., Vinagre, B.M. 2026. Neuromorphic Automatic Reset PI Controller for Simultaneous Anti-Windup and Dead-Zone Compensation: Initial Results. Jornadas de Automática, 47. https://doi.org/10.17979/ja-cea.2026.47.13740

Resumen

La saturación del actuador en sistemas regulados mediante controladores proporcional-integral (PI) provoca el «windup» del integrador y, por tanto, la degradación del rendimiento. Las configuraciones clásicas de control PI con reset automático abordan este problema introduciendo un modelo de saturación que limita la acción integral. En este artículo se propone un esquema de control PI antiwindup basado en control neuromórfico (NC), en el que la saturación convencional se sustituye por una neurona. Este elemento permite cumplir una doble función: gracias a su funcionamiento basado en pulsos, impone de forma inherente la saturación cuando la entrada supera la amplitud de los pulsos, al tiempo que mitiga los efectos de la zona muerta sin requerir un modelado explícito. Al abordar ambas no linealidades mediante un único elemento, la arquitectura de control general se mantiene notablemente simple. Los resultados de simulación en un motor de corriente continua (DC) demuestran la simplicidad y la eficacia de la estrategia propuesta en un actuador no lineal con zona muerta y saturación.

Palabras clave: Modelado de sistemas híbridos y conmutados, Control basado en eventos, Anti-windup, Control de sistemas conmutados.

Neuromorphic Automatic Reset PI Controller for Simultaneous Anti-Windup and Dead-Zone Compensation: Initial Results

Abstract

Actuator saturation in systems regulated by proportional-integral (PI) controllers causes integrator ‘windup’ and, consequently, a deterioration in performance. Conventional PI control configurations with automatic reset address this problem by introducing a saturation model that limits the integral action. This article proposes an anti-windup PI control scheme based on neuromorphic control (NC), in which conventional saturation is replaced by a neuron. This element fulfils a dual function: thanks to its pulse-based operation, it inherently imposes saturation when the input exceeds the pulse amplitude, whilst mitigating the effects of the dead zone without requiring explicit modelling. By addressing both non-linearities through a single element, the overall control architecture remains remarkably simple. Simulation results on a direct current (DC) motor demonstrate the simplicity and effectiveness of the proposed strategy in a non-linear actuator with dead-zone and saturation.

Keywords: Hybrid and switched systems modelling, Event-based control, Anti-windup, Control of switched systems.

1. Introduction

Modern robotics is increasingly moving toward asynchronous, event-driven architectures to bridge the gap between artificial and biological efficiency. At the forefront of this shift is neuromorphic control (NC), a paradigm originating from analog very large-scale integration. Unlike traditional digital controllers tied to a global clock, NC op-

*Autor para correspondencia: ajserranob@unex.es

erates through pulse-type signals that more closely mimic neural spikes. This intrinsic nature offers a robust solution to low-speed control challenges—specifically nonlinear friction—where conventional proportional-integral-derivative (PID) controllers often succumb to the stick-slip phenomenon (Canudas de Wit et al., 1995). By delivering discrete energy bursts, NC ensures the actuator can consistently overcome static friction thresholds (DeWeerth et al., 1991).

While contemporary literature often associates "neuromorphic" with software implementations of deep learning, this work focuses on the hardware-native interpretation: systems where sensors, processors, and actuators communicate via pulses. Recent advances in vision sensors and sensorimotor integration suggest that fully pulse-driven robotic ecosystems can offer latency and power-consumption advantages in suitable event-driven implementations (Yang et al., 2024). However, as these systems transition to practical industrial applications, they encounter the same physical constraints as classical systems—most notably, actuator saturation.

A critical hurdle in any integral-based control law is reset windup. When an actuator reaches its physical limit, the integral term continues to accumulate error, leading to severe transient overshoots, extended recovery times, and potential system instability. Standard literature offers several anti-windup remedies, such as conditional integration (clamping the error) or back-calculation (adjusting the integral state via a feedback loop) (Åström and Hägglund, 2006). While these are well-established for conventional control, their application within the asynchronous, spike-based paradigm of NC remains an open research gap.

We previously enhanced NC robustness using both fractional-order controllers and neurons, and their analog implementations (Serrano-Balbontín et al., 2023, 2024a). More recently, integer-order versions of these event-driven principles were applied to the analysis of DC motors with friction-induced dead-zones (Serrano-Balbontín et al., 2026a) and the high-precision pressure regulation of soft pneumatic actuators (SPAs) (Serrano-Balbontín et al., 2026b). Building on our preliminary research, we previously introduced a novel architecture that replaces the static feedback gains of classical back-calculation with neurons. This bio-inspired approach was benchmarked against traditional anti-windup strategies to evaluate its dynamic response under saturation. Our findings demonstrated that when these neurons are tuned for high-frequency firing, they emulate the behaviour of a standard back-calculation algorithm with high fidelity. The key benefit when adjusting pulse morphology is that increasing spike amplitude or duration enabled the required compensation at a much lower duty cycle. As a result, the controller signal needs fewer recomputations, cutting computational overhead while preserving strong anti-windup protection (Serrano-Balbontín et al., 2024b). Nonetheless such structure was only useful for antiwindup. In this paper, we explore a strategy that is also suitable to mitigate the effect of dead-zones.

While classical literature tends to use nonlinearity-specific control strategies, such as feedforward compensation, friction observer or sliding mode control for dead-zones (Canudas de Wit et al., 1995), and conditional integration, back-calculation or automatic reset configurations for anti-windup (Åström and Hägglund, 2006), this work proposes a scheme that deals with both types of nonlinearities simultaneously by introducing a single nonlinear element to the PI structure. The main advantage of this unified approach over traditional decoupled compensations is that it eliminates the undesired dynamic interactions between independent dead-zone and anti-windup loops. Furthermore, it reduces the controller tuning effort and computational burden, making it advantageous for applications operating on low-cost embedded hardware where structural simplicity and resource constraints are paramount, as well as for fully pulse-driven communication architectures.

The contributions of this paper are: 1) the design of a neuron-based anti-windup strategy that also mitigates the problem of dead-zone simultaneously, 2) a series of implementation recommendations, and 3) simulation results that demonstrate its simplicity and effectiveness.

The remainder of this paper is organized as follows. Section 2 reviews the fundamentals of commonly used silicon neuron models and classical anti-windup strategies. Section 3 introduces the proposed neuron-based anti-windup proportional-integral (PI) control scheme and describes the neuron model employed to regulate the integrator behaviour under saturation. Simulation results are presented in Section 4. Finally, Section 5 summarizes the main conclusions of the work.

2. Fundamentals

Modern control architectures increasingly combine classical control principles with bio-inspired and neuromorphic concepts, motivating a brief review of silicon neuron models and anti-windup strategies for PID controllers operating under actuator constraints.

In classical back-calculation, an additional feedback path is generated by feeding the error between the actual controller output, and the output of the actuator through a gain. This serves to recompute the integral term in the controller and do not have any effect when the actuator does not saturate (Åström and Hägglund, 2006).

The conditional integration structure evaluates whether the actuator is saturated and whether the current control error would drive the actuator further into saturation. If the actuator is not saturated, or if the error helps the controller return from saturation toward the admissible operating range, the PI controller operates in its standard mode. Otherwise, the input to the integrator is forced to zero, effectively suspending the integration action until the controller can recover (Visioli, 2006).

2.1. Neurons

The literature on neuronal modeling ranges from high-fidelity biophysical models to abstracted signal-encoding representations like integral pulse-frequency modulation (IPFM). Within this spectrum lies the hardware-oriented approach of analog circuits, which leverages electronic physics for energy-efficient neuromorphic computation.

In practice, these approaches converge in silicon neurons—the building blocks of neuromorphic systems. Depending on the application, these circuits may be analog, digital, or mixed-signal, ranging from detailed biophysical emulations to simplified spike-based models.

The IPFM neuron-like modulator is a core component of neuromorphic engineering due to its balance between biological relevance and computational simplicity. Its dynamics is described by the following three expressions. The first describes the integration of the input $u(t)$ up to a threshold K_{ti}:

$$s(t) = \int_{t_{k-1}}^{t} u(t)dt < K_{ti} \tag{1}$$

where $s(t)$ is the integrator output, and t_k is the k-th time when $s(t)$ crosses the value K_{ti} ($s(t_k) = K_{ti}$), with t_0 the initial time. The second indicates the reset of the integral at each t_k instant:

$$s(t_k^+) \leftarrow 0 \tag{2}$$

and the third describes the modulator output, which is a pulse train:

$$z(t) = A \sum_{k=1}^{N} [H(t - t_k) - H(t - t_k - t_h)] \tag{3}$$

where A and t_h are the amplitude and width of the pulse, respectively, H is the Heaviside step function, and N is the number of pulses fired during the experiment. If a firing request arrives while a pulse is active, the high state is extended rather than summed, so the neuron remains bounded by A.

Two neurons are required to represent both the positive and negative components of a signed input signal, with each neuron selectively modulating one of these opposing parts. If the control signal has only one polarity, a single neuron is sufficient.

In modulators, the relevant information is contained in the local average value over a period. For convenience, we define the input fraction as $\xi = \bar{u}_k/A$, where $\bar{u}_k$ is the average input in the period k ($t \in [t_{k-1}, t_k]$). The firing frequency of the neuron (f_k) can be deduced from (1)-(3) as a function of the average input $f_k = 1/(t_k - t_{k-1}) = \bar{u}_k/K_{ti}$. If the threshold is set to $K_{ti} = G_N A t_h$, where G_N^{-1} is the neuron gain, then the frequency becomes $f_k = \xi/(G_N t_h)$. With pulse overlap, the average output is $\bar{z}_k = A \min(1, t_h f_k)$, which is approximately linear when $t_h f_k < 1$ and $G_N = 1$, and saturates at A when firing requests overlap.

2.2. Automatic reset

In many practical applications, PI and PID controllers are designed under the assumption that the actuator operates within its linear range. However, during large transients or aggressive reference changes, the control signal may exceed the actuator limits, causing the integrator to accumulate excessive error and leading to windup phenomena. Instead of redesigning the nominal controller, anti-windup techniques preserve the original PI structure while introducing additional mechanisms that act on the integral term whenever saturation occurs.

The automatic reset configuration of a PI (AR-PI) controller employs the interacting form scheme, where the integral part is implemented as a filter in a positive feedback path, as depicted in Figure 1. A saturation block that models the actuator limits is included to constrain the integral action; since the filter tracks the saturated control signal, it reaches a steady state each time saturation occurs, effectively preventing the windup effect. Furthermore, the inherent dynamics of the filter ensure a smooth transition into and out of the saturation regime, avoiding the abrupt discontinuities often found in logic-based anti-windup schemes. In contrast to conditional integration, where the integrator action is completely suspended, the automatic reset configuration allows the integrator to evolve in a controlled manner.

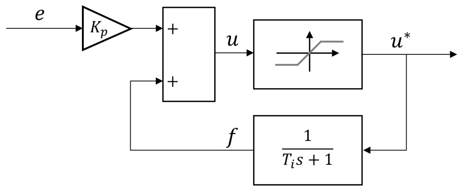

Figure 1: Conventional PI controller in automatic reset configuration.

The corresponding control law is:

$$U^*(s) = \text{sat}_{u_{lim}}\left(K_p E(s) + \frac{1}{T_i s + 1} U^*(s)\right) \tag{4}$$

where u_{lim} is the actuator limit and $\text{sat}_a(.)$ is the saturation function:

$$\text{sat}_a(x) = \begin{cases} x & \text{if } |x| < a \\ a\,\text{sign}(x) & \text{if } |x| \geq a \end{cases} \tag{5}$$

in which a is the saturation threshold and sign(.) is the sign function. When the control signal remains below the saturation threshold ($u^*(t) = u(t)$), it exhibits behavior equivalent to that of a conventional PI controller:

$$U^*(s) = \frac{K_p E(s)}{1 - \frac{1}{T_i s+1}} = K_p \left(\frac{T_i s + 1}{T_i s}\right) E(s) = K_p \left(1 + \frac{1}{T_i s}\right) E(s) \tag{6}$$

When the threshold is surpassed, let $u(t) = K_p e(t) + f(t)$ denote the signal before the saturation block. The saturated controller output is then

$$u^*(t) = u_{lim}\,\text{sign}(u(t)), \tag{7}$$

For the positive saturation case, the output of the filter evolves as:

$$F(s) = \frac{1}{T_i s + 1} \frac{u_{lim}}{s} + \frac{T_i}{T_i s + 1} f_0 \tag{8}$$

where f_0 is the filter output at the moment at which saturation commences. For the negative saturation case, the same expression holds by replacing u_{lim} with $-u_{lim}$. In the time domain:

$$f(t) = u_{lim} + (f_0 - u_{lim}) e^{-\frac{t}{T_i}} \tag{9}$$

In this configuration, the constant T_i has two roles: it defines the integral gain within the linear operating range and determines the rate at which the controller recovers from saturation by dissipating the accumulated error.

3. Neuromorphic Automatic Reset PI Controller

The control scheme proposed in this work is based on the classical automatic reset configuration of a PI controller presented in the previous section. In the proposed approach, the conventional saturation element is replaced by a neuron, since neurons intrinsically exhibit a saturating behavior due to their inability to generate output signals with amplitudes exceeding the pulse amplitude A as shown in Fig. 2. Additionally, by introducing the neuron in this specific configuration rather than in others, such as back-calculation, we can take advantage of the pulses to address the dead zone—interested readers may refer to our previous work on neuron-based back-calculation (Serrano-Balbontín et al., 2024b).

It should be noted that a variant of the automatic reset scheme exists where saturation is placed in the feedback path. However, by positioning the neuron there, the controller output ceases to be a pulse train. Consequently, the neuron ability to compensate for the dead-zone is lost. We therefore adhere to the previously proposed scheme.

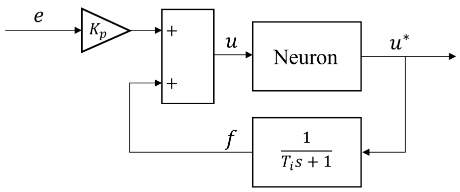

Figure 2: Neuromorphic PI controller in automatic reset configuration.

Unlike classical AR-PI, the neuromorphic counterpart (henceforth, AR-NPI) always takes one of three states corresponding to the signed control signal of the positive/negative IPFM pair:

$$u^*(t) = z^+ - z^- \in \{-A, 0, A\} \tag{10}$$

where z^+ and z^- are the outputs of the positive and negative neurons, respectively. Nonetheless, the neurons generate a signal that directly represents their input. As described in Section 2, this representation is approximately linear in average when $t_h f_k < 1$, while it saturates at A when firing requests overlap. Consequently, on an average basis, it approximates the continuous case where saturation occurs at the value A:

$$U(s) \approx \mathrm{sat}_A\left(K_p E(s) + \frac{1}{T_i s + 1} U(s)\right) \tag{11}$$

The assumption of average behavior is suitable when the firing frequency is high enough so that the distortion on the signal is minimal and harmonics are easily filtered. In the comparisons reported in this work, these limits are selected as $A = u_{lim} = V_{sat}$, where V_{sat} denotes the physical saturation limit of the actuator, so that the AR-NPI reproduces the same saturation level as the classical AR-PI controller. With this choice, the tuning of pulse width t_h determines the smoothness of the feedback signal.

Figure 3 depicts the closed-loop configuration employed to control the output of a system that simultaneously exhibits actuator saturation and dead-zone nonlinearities, which constitute two of the most frequently encountered classes of nonlinear behavior in control systems.

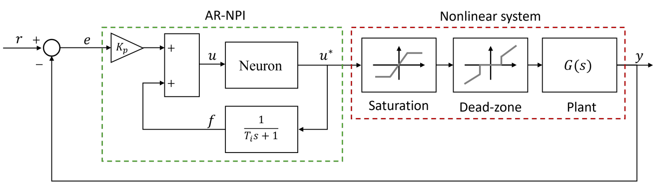

Figure 3: Closed-loop configuration with AR-NPI controller, actuator saturation and dead-zone nonlinearity.

3.1. Considerations for controller tuning

The neuron is designed to surpass dead-zone and simultaneously act as the saturation model in the reset configuration. Then, the parameters are tuned based on the following deductions:

- Each pulse produces an increment in the output proportional to the product At_h (area of the pulse). Then, there is a compromise between A and t_h that determines the precision.
- The pulse amplitude A must be large enough to overcome the dead-zone and, for exact comparison with the classical automatic-reset PI, is set equal to the reset and actuator limits, $A = u_{lim} = V_{sat}$. Choosing $A < V_{sat}$ is also possible as a design trade-off to reduce pulse amplitude or increase precision, but in that case the neuromorphic reset loop saturates before the physical actuator and no longer emulates the same limit as the AR-PI benchmark.
- Increasing t_h worsens the precision, and must be a multiple of the sampling time.
- In order to produce a unitary gain of the neuron, the threshold must be equal to $K_{ti} = At_h$, which enables to reproduce the controller signal faithfully.

The main linear controller, typically a PID controller, is designed by using classical methods by considering that the nonlinearities are fully compensated.

4. Application example

4.1. Nonlinear system

The plant under consideration is a DC motor, its linear dynamics are represented by a second-order transfer function:

$$G(s) = \frac{\theta(s)}{V(s)} = \frac{K}{\tau s^2 + s} \tag{12}$$

where θ is the position, K is the motor gain, and τ is the time constant, and $v(t)$ is the effective voltage applied to the motor after input saturation and a symmetric dead-zone:

$$v(t) = \begin{cases} 0, & \text{if } |v_{in}| \le |V_{dz}|, \\ v_{in} - V_{dz}\,\mathrm{sign}(v_{in}), & \text{if } |V_{dz}| < |v_{in}| < |V_{sat}|, \\ (V_{sat} - V_{dz})\,\mathrm{sign}(v_{in}), & \text{if } |v_{in}| \ge |V_{sat}|. \end{cases} \tag{13}$$

where $v_{in}(t) = u^*(t)$ is the voltage command delivered by the controller to the actuator before the actuator nonlinearity, and V_{dz} and V_{sat} are the dead-zone threshold and the input saturation limit, respectively. Thus, the maximum effective voltage applied to the plant is $V_{sat} - V_{dz}$.

This example is given only to examine how integral action affects tracking performance under nonlinear conditions. Although integral action may seem unnecessary for ideal position regulation, it is included in the position control loop to guarantee zero steady-state error under load disturbances and to enable accurate tracking of more general reference signals. The analysis extends directly to speed control problems.

4.2. System and controller parameters

The parameters were selected for illustrative purposes as follows:

- System parameters: The plant parameters are chosen as $K = 30$ rad s^{-1}V^{-1}, $\tau = 0.13$ s, $V_{dz} = 0.2$ V, and $V_{sat} = 0.5$ V, aiming to represent the characteristics of a low-cost DC motor.
- PI controller: The controller gains are set to $K_p = 0.8$ and $T_i = 0.4$ s. These values are intentionally selected to induce a significant overshoot, thereby clearly highlighting the transient response differences and limitations of each control strategy.
- Neuron: The neuron is configured to model the saturation block with $A = V_{sat} = 0.5$ V, while the pulse width is set to $t_h = 0.1$ ms to ensure a smooth control action.

4.3. Simulation results

To elucidate the operating principles of the conventional AR-PI controller and the AR-NPI controller, the corresponding simulation results are presented next.

Initially, only a saturating nonlinearity with a threshold of 0.5 V was incorporated into the simulations, thereby enabling the isolated examination of a single phenomenon at a time. The neuron was configured to operate at high frequency, ensuring the validity of the averaging assumption and minimizing the introduction of distortion.

In Figure 4, the controller output, ($u^*(t)$), the filter output, ($f(t)$), and the sum block output, ($u(t)$), are shown for both the AR-PI and AR-NPI controllers. A marked difference in the controller outputs can be observed: whereas the classical controller generates a continuous and smooth control signal, the neuromorphic implementation yields a pulsed output sequence, effectively constraining the controller to operate in three discrete states. However, the filter outputs produced by both controllers are nearly indistinguishable, thereby demonstrating the capability of the neuron to faithfully reproduce the input signal $u(t)$. Hence, it is expected to observe the same antiwindup capabilities for the proposed scheme.

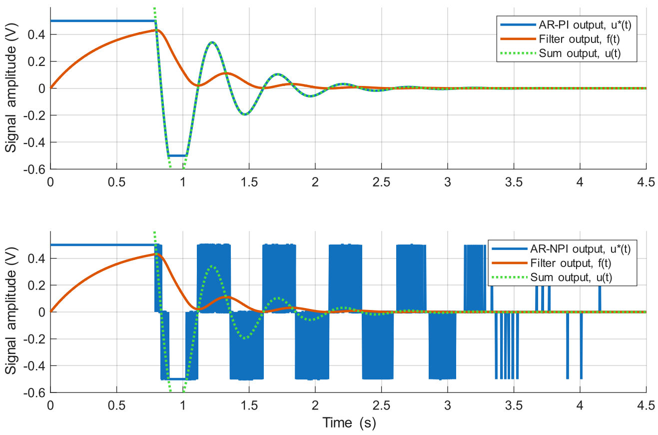

Figure 4: Controller output $u^*(t)$ (blue), filter output $f(t)$ (orange) and sum block output $u(t)$ (green) for classical AR-PI controller (top) and AR-NPI controller (bottom). Dead-zone was not considered.

Figure 5 shows controller signals for two tuned AR-NPI controllers. The first corresponds to the case shown in the previous figure (AR-NPI 1), while the second is a less smooth version of the first (AR-NPI 2), with an increased pulse width of the neuron by a factor of 100. It is possible to observe that AR-NPI 2 produces fewer pulses to encode the same signal, which directly implies a lower switching effort because fewer switching events are required. On the other hand, the output of the filter is less smooth as observed in the zoom in view.

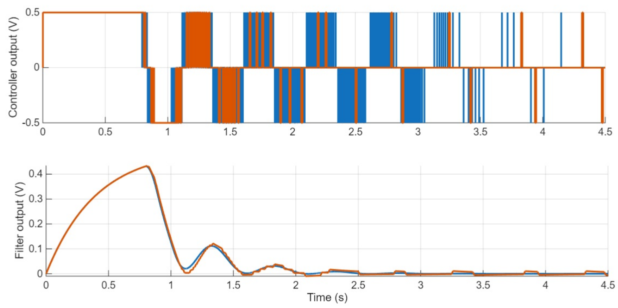

Figure 5: Controller output, $u^*(t)$ (top) and filter output, $f(t)$ (bottom) for AR-NPI controllers, AR-NPI 1 with $t_h = 0.1$ ms (blue) and AR-NPI 2 with $t_h = 10$ ms (orange). Dead-zone was not considered.

Figure 6 shows the system output for both controllers of the same simulation shown in the previous figure. A zoom in of the AR controllers is included to observe the subtle deviation in amplitude caused by the less smooth neuron of the AR-NPI 2 controller. The results validate the anti-windup capabilities of the AR-NPI controller. This serves as proof of the first of the two purposes of the scheme.

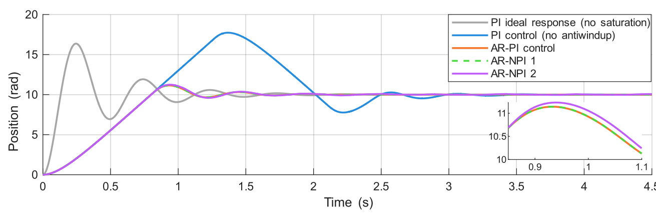

Figure 6: System output for the PI controller in ideal conditions, no saturation (gray), PI controller without antiwindup in presence of saturation (blue), AR-PI controller (orange), AR-NPI 1 controller (green) and AR-NPI 2 controller (purple). Dead-zone was not considered.

Now consider only a dead-zone nonlinearity with a threshold equal to 0.2 V. Figure 7 shows the system responses obtained using both the AR-PI and the AR-NPI controllers. The AR-NPI controller exhibits a tracking behavior that closely approximates the ideal response (i.e., the response in the absence of a dead-zone), with only minor deviations. In contrast, the performance of the classical AR-PI controller is significantly degraded by the presence of the dead-zone, resulting in an increased rise time and an overshoot that deviates from the specification established for the ideal controller, as well as distortions clearly attributable to nonlinear effects. Hence, the second purpose of the neuron is demonstrated.

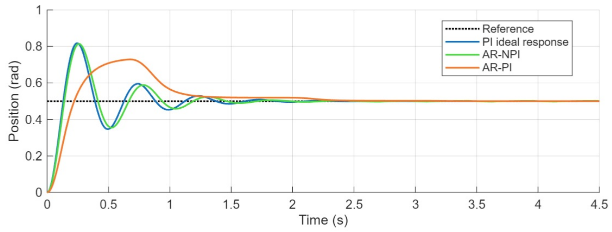

Figure 7: System output for the PI controller in ideal conditions, no dead-zone (blue), the AR-PI controller (orange), and the AR-NPI controller (green). Saturation was not considered.

Having independently validated the two objectives, tests are subsequently conducted to evaluate the controller under operating conditions in which both nonlinearities are simultaneously present (V_{sat} = 0.5 V, and V_{dz} = 0.2 V).

Figure 8 illustrates the performance advantages of the AR-NPI controller when both nonlinearities are taken into account. Although the AR-NPI response exhibits some deviation due to the presence of the dead zone, its behavior remains approximately linear. In contrast, the AR-PI response becomes significantly distorted, and the settling time increases substantially. The neuromorphic controller significantly outperforms the continuous approach, achieving an integral time absolute error (ITAE) of 0.1104 versus 0.3526. Notably, it also reduces the integral absolute control signal (IACS) from 0.7463 to 0.2005. A comparison using performance indices demonstrates that the neuromorphic structure not only enhances tracking precision but also optimizes control effort. The elevated IACS in the continuous controller indicates erratic or excessive control activity that fails to improve precision, reflecting an inefficient management of the control effort.

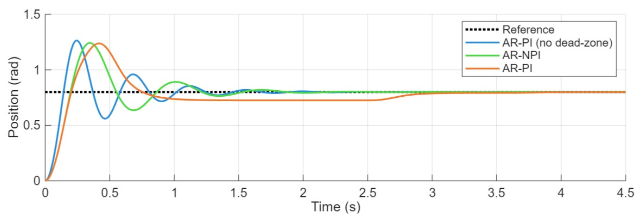

Figure 8: System output for the PI controller in ideal conditions (blue), the AR-PI controller (orange), and the AR-NPI controller (green). Both nonlinearities were considered simultaneously.

5. Conclusions

This paper has presented preliminary results towards a novel neuromorphic anti-windup proportional-integral (PI) control scheme. By replacing the conventional saturation element in an automatic reset configuration with a single neuromorphic element, the proposed architecture offers a unified and remarkably simple solution to two common nonlinearities: actuator saturation and dead-zone. Simulation results obtained confirmed the dual purpose of the neuron in the closed loop, demonstrating that its intrinsic pulse-based operation effectively prevents integrator windup when limits are exceeded, while simultaneously delivering discrete energy bursts to mitigate dead-zone effects without requiring explicit modelling. Future work will involve a more in-depth theoretical analysis of this dual-purpose control strategy, as well as an analysis of the controller robustness and energy efficiency.

Agradecimientos

This research was funded by the Agencia Estatal de Investigación (Ministerio de Ciencia e Innovación) through project PID2022-141409OB-C22/AEI/10.13039/501100011033/FEDER, UE, by the Junta de Extremadura through grant GR24059 within “Ayudas a Grupos de Investigación”, and by the European Regional Development Fund (FEDER) “A way to make Europe”.

Andrés Serrano would like to thank the Ministerio de Ciencia, Innovación y Universidades for its support through the scholarship no. FPU22/00885 of the FPU Program.

References

Åström, K., Hägglund, T., 2006. Advanced PID Control. ISA - The Instrumentation, Systems and Automation Society.

Canudas de Wit, C., Olsson, H., Astrom, K., Lischinsky, P., 1995. A new model for control of systems with friction. IEEE Transactions on Automatic Control 40 (3), 419–425.
DOI: 10.1109/9.376053

DeWeerth, S., Nielsen, L., Mead, C., Astrom, K., 1991. A simple neuron servo. IEEE Transactions on Neural Networks 2 (2), 248–251.
DOI: 10.1109/72.80335

Serrano-Balbontín, A. J., Mérida, L., Vinagre, B. M., Feliu-Batlle, V., Tejado, I., 2026a. Neuromorphic control of DC motors with static friction-dominated dynamics. IEEE Transactions on Control Systems Technology (In Press).
DOI: 10.1109/TCST.2026.3698162

Serrano-Balbontín, A. J., Tejado, I., Mancha-Sánchez, E., Vinagre, B. M., 2023. Introducing fractional order dynamics in neuromorphic control: application to a velocity servomotor. In: 2023 European Control Conference (ECC). pp. 1–6.
DOI: 10.23919/ECC57647.2023.10178322

Serrano-Balbontín, A. J., Tejado, I., Vinagre, B. M., 2024a. Field-programmable analog array implementation of neuromorphic silicon neurons with fractional dynamics. Fractal and Fractional 8 (4).
DOI: 10.3390/fractalfract8040226

Serrano-Balbontín, A. J., Tejado, I., Vinagre, B. M., 2024b. A neuron-based back-calculation anti-windup strategy: First results. IFAC-PapersOnLine 58 (7), 388–393.
DOI: 10.1016/j.ifacol.2024.08.093

Serrano-Balbontín, A. J., Tejado, I., Vinagre, B. M., Aphale, S. S., San-Millan, A., 2026b. Spiking control of a solenoid valve for high-precision pressure regulation in soft robotics. IEEE Control Systems Letters 10, 127–132.
DOI: 10.1109/LCSYS.2026.3672133

Visioli, A., 2006. Practical PID control. Springer London.
DOI: 10.1007/1-84628-586-0

Yang, Y., Zhu, F., Zhang, X., Chen, P., Wang, Y., Zhu, J., Ding, Y., Cheng, L., Li, C., Jiang, H., Wang, Z., Lin, P., Shi, T., Wang, M., Liu, Q., Xu, N., Liu, M., May 2024. Firing feature-driven neural circuits with scalable memristive neurons for robotic obstacle avoidance. Nat. Commun. 15 (1), 4318.